Rev. Roum. Sci. Techn.– Électrotechn. et Énerg.
Vol. **71**, *1*, pp. 3–8, Bucarest, 2026

DESIGN SENSITIVITY ANALYSIS AND PERFORMANCE IMPROVEMENT OF A SIX-PHASE SQUIRREL-CAGE INDUCTION MACHINE

YACINE BENDJEDDOU[1], ABDELLATIF SEGHIOUR[1], MUSTAPHA TAIB[1], HEMZA SELLAMNA[1], TERTAG ABDELKADER[1], NOUREDDINE BENOUZZA[2]

Keywords: Efficiency; Loss minimization; Motor mass reduction; Performance enhancement; Power output maximization; Reliability; Six-phase induction motor.

Current research increasingly focuses on improving the design of six-phase induction motors, particularly within the realm of scientific inquiry. The primary objectives of this study include maximizing motor efficiency while minimizing losses, decreasing motor mass, maximizing power output within a compact size, addressing environmental concerns such as vibrations, acoustic noise, electromagnetic compatibility, and incorporating eco-friendly materials. This paper investigates the design sensitivity analysis and performance improvement of six-phase asynchronous motors under investigation. To achieve this goal, design parameter variations are performed to analyze their influence on machine characteristics, geometric and electrical parameters, aiming to minimize losses and motor size while maximizing efficiency. This approach endeavors to create robust and dependable machines while minimizing associated costs.

1. INTRODUCTION

The rapid development of industrial systems and electric propulsion technologies has increased the demand for high-performance, reliable, and efficient electrical machines. In this context, multiphase induction machines, and particularly the six-phase double-star induction machine (DSIM), have attracted growing attention due to their enhanced fault tolerance, reduced torque pulsations, lower harmonic content, and superior efficiency compared to traditional three-phase counterparts [1,2]. Designing such machines requires a deep understanding of how electrical and geometrical parameters influence overall performance, losses, and cost. While many studies have applied mathematical optimization techniques to improve machine efficiency and torque characteristics [3,4], an equally critical step lies in conducting a design sensitivity analysis. This approach identifies the most influential parameters before attempting a formal optimization, ensuring that subsequent optimization procedures are both effective and physically meaningful.

The present work, therefore, focuses on the design sensitivity analysis of a 0.75 kW six-phase squirrel-cage induction machine using ANSYS Maxwell. By varying key design parameters such as current density, air gap, and slot geometry, the study evaluates their impact on torque, starting current, losses, and efficiency. The results provide valuable insight into how small variations in design choices affect machine behavior, paving the way for more advanced optimization strategies in future research.

2. PRESENTATION OF THE MACHINE

The magneto-thermal analysis of the double-star machine performed using the ANSYS Maxwell software encompasses the following electrical parameters:

Table I

Parameters of the DSIM

Symbol	Quantity	Value
P	rated power	0.75 kW
U_n	rated voltage	150 V
I_n	rated current	2.8 A
T_n	rated torque	7.91 N.m
Ω_n	rated rotational speed	905 rpm
F	frequency	50 Hz
M	number of phases	6
P	number of poles	6
S_s	number of slots	36
S_r	number of rotor bars	33

3. THE CONSTRUCTION OF THE WINDING OF THE 750W DOUBLE-STAR MACHINE

The winding of the DSIM is single-layered, distributed in a concentric manner, and has 6 poles. The number of slots per pole and per phase is q = 1. Each phase contains 366 turns, meaning each coil comprises 122 turns.

Fig. 1 – Double-star squirrel-cage asynchronous motor 0.75 kW.

The phase distribution in the slots used in the DSIM simulation is as follows:

Table 2

The connections of the slots in the six phases of the DSIM.

Currents direction	Phase A	Phase B	Phase C	Phase D	Phase E	Phase F
	Slot numbering					
+	1	5	9	2	6	10
-	7	11	15	8	12	16
+	13	17	21	14	18	22
-	19	23	27	20	24	28
+	25	29	33	26	30	34
-	31	35	3	32	36	4

[1] Laboratoire de génie électrique et de matériaux, École supérieure en génie électrique et énergétique d'Oran, 31000, Algérie.
[2] Université des sciences et technologies d'Oran, USTO, 31000, Algérie.
E-mails : bendjeddou_yacine@esgee-oran.dz, seghiour_abdellatif@esgee-oran.dz, taib_mustapha@esgee-oran.dz, sellamna_hemza@esgee-oran.dz, benouza@yahoo.com

DOI: 10.59277/RRST-EE.2026.1.1

4. MAXWELL 2D AND ANSYS

ANSYS Maxwell represents an economical electromagnetic field simulation software, specifically designed for designers involved in the development and analysis of electromagnetic and electromechanical devices in 3D and 2D, such as motors, actuators, transformers, sensors, and coils. Maxwell 2D stands out as a highly performant bilateral toolkit that leverages finite element analysis (FEA) to address challenges related to electrical, magnetostatic [5], eddy current, and transient aspects. By applying Maxwell's equations within a defined space, Maxwell 2D accurately resolves electromagnetic field problems, incorporating relevant materials, boundary conditions, and source parameters specified by the model [6,7]. The differential forms of Maxwell's equations are expressed as follows [9–11]:

• Maxwell-Gauss equation

$$\mathrm{div}\vec{D} = \zeta \quad (1)$$

• Maxwell-Faraday equation

$$\mathrm{rot}\vec{E} = -\frac{\partial \vec{B}}{dt}. \quad (2)$$

• Conservation of magnetic flux equation

$$\mathrm{div}\vec{B} = 0, \quad (3)$$

• Maxwell-Ampere equation

$$\mathrm{rot}\vec{H} = \vec{j} + \frac{\partial \vec{D}}{\partial t}. \quad (4)$$

5. RESULTS AND INTERPRETATION

The mapping of the distribution of magnetic induction field lines in the DSIM, as depicted in Fig. 2, demonstrates that the machine has six poles. Furthermore, the induction values approximately align with the values injected into the first magnetization curve. Figures 3 and 4 illustrate the electrical and mechanical characteristics of the motor, demonstrating how the electromagnetic and efficiency vary with the motor's rotational speed. We studied the behavior of the DSIM under load, powering the motor in a star configuration with a voltage of 150V between phases and loading it with a load equivalent to its nominal torque. One of the major issues encountered during the startup of asynchronous machines is the high starting current, also known as the startup current. When an asynchronous machine starts, it requires a relatively high amount of current to overcome the rotor's inertia and establish a magnetic field in the stator windings. This startup current can be several times higher than the machine's nominal operating current.

The waveform developed under the excitation of the double-star motor is represented up to 300 ms for clarity. As shown in Fig. 5, the motor draws a peak starting current of 12 A, which corresponds to an RMS value of approximately 8.49 A. After around 100 ms from the start of the simulation, the current stabilizes at a lower peak value of 4 A, equivalent to an RMS value of approximately 2.8 A.

The torque curve over time for our machine DSIM, illustrated in Fig. 6, reaches a high value of 32 Nm at startup, then stabilizes at an average of 8 Nm with fluctuations. This torque value is necessary to accelerate the rotor and overcome friction and inertia forces, ensuring that the machine quickly reaches its nominal operating speed, as shown in Fig. 7. Figure 8 shows that the machine has a six-pole skewed induction. This ripple is due to space harmonics caused by the non-uniform geometry of the machine and the materials used in the construction of the stator and rotor.

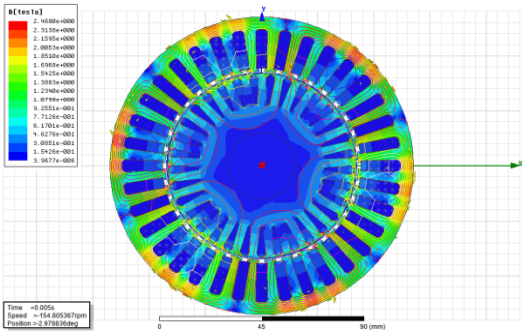

Fig. 2 – Dual star induction machine magnetic field distribution.

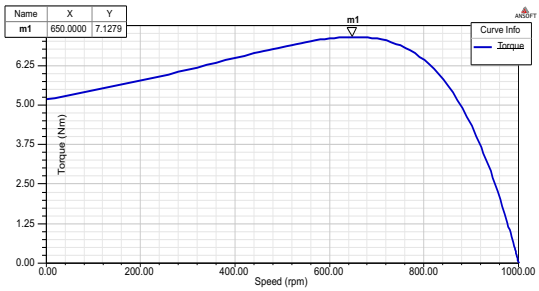

Fig. 3 – The electromagnetic torque as a function of speed.

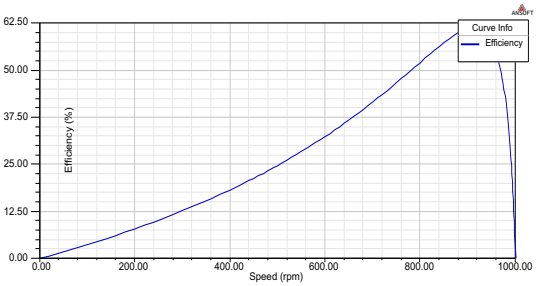

Fig. 4 – The efficiency of the machine as a function of speed.

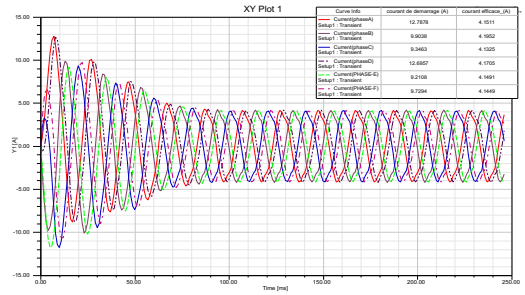

Fig. 5 – The curve of DSIM phase currents as a function of time.

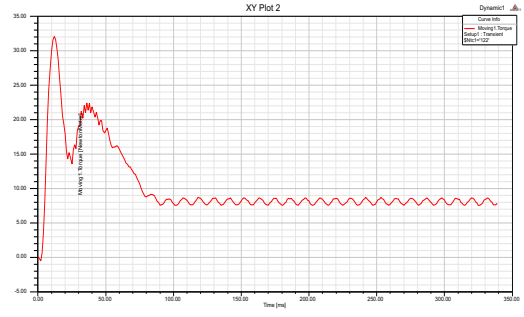

Fig. 6 – The torque curve as a function of time.

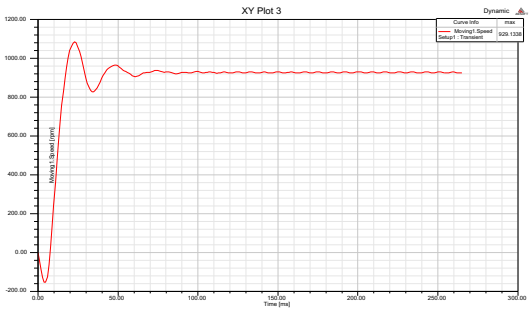

Fig. 7 – The curve of rotational speed as a function of time.

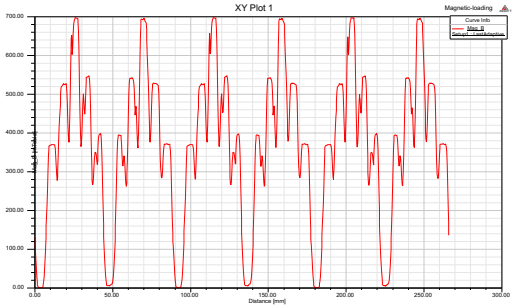

Fig. 8 – Distribution of magnetic induction in the air gap.

5.1 DESIGN SENSITIVITY ANALYSIS OF THE DSIM

In this section, electrical and geometric parameters such as current density, linear load, and conductor dimensions (windings) are varied to study their impact on performance. The analysis aims to identify parameter combinations that yield improved torque, reduced starting current, and enhanced efficiency. The design parameters of the existing DSIM:

Table 3

The results of the parameters found for the existing DSIM.

Parameter	Quantity
rated power	0.75 kW
power factor	0.75 A/cm
linear load	456.46
current density	9 A/mm²
nominal current	2.8 A
conductor diameter	0.63 mm
conductor cross-sectional area	0.311 mm²
notch section	64 mm²
wire fill factor in the slot	0.6
wire resistivity at 80°C	$2.17 \cdot 10^{-8}\,\Omega$
aluminum resistivity at 80°C	$3.1 \cdot 10^{-8}\,\Omega$
ring thickness	17 mm
mechanical losses	6.22 W
Joule losses	248.66 W
iron losses	161 W
total losses	416.38 W
rated torque	7.91 N.m
efficiency	64.30%

5.1.1 THE FIRST CASE

In the first case, the analysis resulted in a reduction of both the winding and aluminum bar temperatures, leading to lower electrical resistivity at 20°C.

Table 4

The results found in the first case.

Parameter	Quantity
rated power	0.75 kW
power factor	0.75 A/cm
linear load	456.469 A/mm²
current density	9 A/mm²
nominal current	2.8 A
conductor diameter	0.63 mm
conductor cross-sectional area	0.311 mm²
notch section	64 mm²
wire fill factor in the slot	0.6
wire resistivity at 80°C	$1.724 \cdot 10^{-8}\,\Omega$
aluminum resistivity at 80°C	$2.82 \cdot 10^{-8}\,\Omega$
ring thickness	17 mm
mechanical losses	6.22 W
Joule losses	212.07 W
iron losses	161 W
total losses	373.07 W
rated torque	7.91 N.m
efficiency	66.78%

5.1.2 THE SECOND CASE

In the second case, the variations are the diameter of the copper wire used in winding both stators, and the end ring diameter 'De'.

Table 5

The results found in the second case.

Parameter	Quantity
rated power	0.75 kW
power factor	0.75 A/cm
linear load	456.46
current density	7.95 A/mm²
nominal current	2.8 A
conductor diameter	0.67 mm
conductor cross-sectional area	0.352 mm²
notch section	71.57 mm²
wire fill factor in the slot	0.6
wire resistivity at 80°C	$2.17 \cdot 10^{-8}\,\Omega$
aluminum resistivity at 80°C	$3.1 \cdot 10^{-8}\,\Omega$
ring thickness	14 mm
mechanical losses	72 W
Joule losses	232.94 W
iron losses	148.93 W
total losses	388.59 W
rated torque	7.91 N.m
efficiency	65.87%

When changing the wire diameter with the ring diameter, we observe:

• A reduction in losses improves the efficiency of the DSIM.

• For a fixed nominal current of 2.8 A and a conductor diameter of 0.67 mm, the current density decreases to 7.95 A/mm².

• The notch section increases from 64 mm² to 71.57 mm², which reduces iron losses.

• Increasing the size of the copper conductor leads to an increase in machine cost.

5.1.3 THE THIRD CASE

Regarding the third case, the variables are the stator current density J_s, the current density in the rotor bars J_b, and in the end ring J_e. At the same winding temperature, the results are as follows:

Table 6

The results found in the third case.

Parameter	Quantity
rated power	0.75 kW
power factor	0.75 A/cm
linear load	456.46 A/cm
current density	7.5 A/mm²
nominal current	2.8 A
conductor diameter	0.69 mm
conductor cross-sectional area	0.373 mm²
notch section	75.84 mm²
wire fill factor in the slot	0.6
wire resistivity at 80°C	$2.17 \cdot 10^{-8}\,\Omega$
aluminum resistivity at 80°C	$3.1 \cdot 10^{-8}\,\Omega$
ring thickness	17 mm
mechanical losses	6.72 W
Joule losses	216.92 W
iron losses	142.08 W
total losses	365.64 W

rated torque	7.91 N.m
efficiency	67.22%

The modification of the stator current density Js affects the conductor's cross-section, leading to an increase in the stator slot cross-section and a reduction in the weight of the stator teeth, thus reducing iron losses. Due to the decrease in current density in the machine conductors, we observe a reduction in resistance, resulting in a decrease in the machine's operating temperature. Consequently, Joule losses decrease, leading to an improvement in machine efficiency. Adjusting the current densities J_b and Je reduces losses in the bars and in the ring, thereby improving the motor's efficiency. The main drawback of these modifications lies in the increased weight of the machine, resulting in higher manufacturing costs.

5.1.3 THE FOURTH CASE

In this case, we aim to modify the linear load, and to do so, we need to adjust the number of turns. The results found are as follows:

Table 7

The results found in the fourth case.

Parameter	Quantity
rated power	0.75 kW
power factor	0.75 A/cm
linear load	390 A/cm
current density	9 A/mm²
nominal current	2.8 A
conductor diameter	0.63 mm
conductor cross-sectional area	0.312 mm²
notch section	64 mm²
wire fill factor in the slot	0.51
wire resistivity at 80°C	$2.17 \cdot 10^{-8}\,\Omega$
aluminum resistivity at 80°C	$3.1 \cdot 10^{-8}\,\Omega$
ring thickness	17 mm
mechanical losses	6.72 W
Joule losses	211.3 W
iron losses	161 W
total losses	379.02 W
rated torque	7.91 N.m
efficiency	66.42%

In summary, by decreasing the linear load, we achieve the following benefits: reduced heating, increased overload capacity, lesser copper usage, and decreased Joule losses.

5.2 PERFORMANCE EVALUATION USING ANSYS MAXWELL SOFTWARE

The ANSYS Maxwell-based simulations demonstrate the effectiveness of the parameter sensitivity approach. Adjusting parameters such as the air gap, stator outer and inner diameters, and slot geometry revealed substantial effects on starting current, torque, and efficiency. For instance, a reduced air gap thickness led to improved torque while maintaining acceptable loss levels.

The analysis highlights that by tuning specific design variables, efficiency improvements of up to 5% can be achieved without additional manufacturing complexity.

Table 8

The results found for the existed DSIM

Parameter	Quantity
outer diameter of the stator D_{ext}	146 mm
inner diameter of the stator D_{int}	85.8 mm
air gap	1.08 mm
maximum slot width b_{s2}	6.03 mm
minimum slot width b_{s1}	4.7 mm
conductor cross-sectional area S_{co}	0.312 mm
stator slot opening b_{s0}	2.4 mm
key height h_k	0.5 mm
slot wedge height h_f	0.8 mm
effective slot height h_{ench}	17.94 mm
height of rotor bars	13.5 mm
nominal current, Ansys	2.91 A
starting current / nominal current	12.78
rated torque	7.98 Nm
starting torque	36.01 Nm
starting torque / rated torque	4.51
rated speed	919 rpm
Joule losses	256.76 W
iron losses	161.61 W
mechanical losses	6.91 W
total losses	425.28 W
efficiency	63.81%

5.2.1 THE FIRST CASE

In this case, we aim to modify the outer diameter of the stator from 140 mm to 146 mm. The results after the variation in the first case are as follows:

Table 9

The results found for the first case by ANSYS

Parameter	The actual value of the machine	The improved values
rated current, Ansys	2.91 A	2.68 A
starting current	12.78 A	12.2 A
rated torque	7.98 N.m	8.2 N.m
starting torque	36.01 N.m	37 N.m
starting torque/rated torque	4.51	4.51
rated rotating speed	919 rpm	917 rpm
Joule losses	256.76 W	226.4 W
iron losses	161.61 W	161 W
mechanical losses	6.91 W	6.91 W
total losses	425.28 W	394.33 W
efficiency	63.81%	65.5 %

During this change in the external diameter of the stator, we observe:

- Decrease in starting current from 12.78 A to 12.2 A and in nominal current.
- Increase in starting torque and nominal torque of the machine.
- The reduction in Joule losses leads to a decrease in total losses, resulting in an improvement in the machine's efficiency.

5.2.2 THE SECOND CASE

In this case, the variation concerns the air gap thickness, changing from g=1.08 mm to g=0.5 mm. The results found are as follows:

Table 10

The results found in the second case by ANSYS.

Parameter	The actual value of the machine	The improved values
rated current, Ansys	2.91 A	2.54 A
starting current	12.78 A	12.83 A
rated torque	7.98 N.m	8.05 N.m
starting torque	36.01 N.m	37.3 N.m
starting torque/rated torque	4.51	4.63
rated rotating speed	919 rpm/min	921.44 rpm
Joule losses	256.76 W	221.38 W
iron losses	161.61 W	161 W
mechanical losses	6.91 W	6.96 W
total losses	425.28 W	389.34 W
efficiency	63.81%	65.85 %

We observe an increase in the starting torque as well as an increase in the starting current. However, a decrease in iron losses leads to a reduction in motor heating and promotes good efficiency. The efficiency of the machine studied in this theoretical study reaches an improved value of 65.85%.

5.2.3 THE THIRD CASE

In this case, the variation concerns the inner diameter of the machine, which changes from 85.8 to 82 mm. The results found are as follows:

Table 11

The results found in the third case by ANSYS.

Parameter	The actual value of the machine	The improved values
rated current, Ansys)	2.91 A	2.82 A
starting current	12.78 A	11.79 A
rated torque	7.98 N.m	7.98 N.m
starting torque	36.01 N.m	36.08 N.m
starting torque/rated torque	4.51	4.52
rated rotating speed	919 rpm/min	903.18 rpm
Joule losses	256.76 W	245.38 W
iron losses	161.61 W	151.54 W
mechanical losses	6.91 W	6.69 W
total losses	425.28 W	403.61 W
efficiency	63.81%	65.01 %

During this change in the inner diameter of the stator, we observe:

- A decrease in nominal current and starting current.
- The starting torque remains almost the same.
- The reduction in Joule losses and iron losses ensures an improvement in the machine's efficiency.

5.2.4 THE FOURTH CASE

In this case, we attempt to modify the conductor cross-sectional area used in the stator winding of the machine for the following two sections:

- For the section S_{co}=0.283mm² Z_s=135;
- For the section S_{co}=0.353mm² Z_s=108.

Table 12

The results from the fourth case in ANSYS.

Parameter	Sco=0.283mm²	Sco=0.353mm²
rated current (In)	2.47 A	3.63 A
starting current	11.24 A	14.55 A
rated torque	7.945 N.m	8.16 N.m
starting torque	34.40 N.m	37.8 N.m
rated rotating speed	900.35 tr/min	933.15 rpm
Joule losses	237.56 W	279.46 W
iron losses	161.61 W	161 W
mechanical losses	6.66 W	7.15 W
total losses	405.83 W	447.61 W
efficiency	64.88%	62.62 %

When the conductor section is smaller than the machine's reference section, it results in a decrease in nominal current, starting current, nominal torque, and starting torque compared to their original values. However, this is accompanied by a reduction in Joule losses and mechanical losses, leading to a slight increase in machine efficiency. Conversely, if the conductor section is increased to S_{co}=0.353, a higher starting current and a higher starting torque are observed than the reference values. However, this leads to a decrease in machine efficiency.

Among the two cases examined in this analysis, it is observed that the case where the section is reduced is better than the other, but it results in a slight decrease in starting torque, which poses a problem during motor startup.

5.2.4 THE FIFTH CASE

In this case, the modification of the machine's geometry affects stator parameters such as the maximum slot width b_{s1}, the minimum slot width b_{s2}, the slot wedge height, the effective slot height, and the stator slot opening b_{s0}, which successively take the following values: 6.14 mm, 4.37 mm, 2 mm, 13 mm.

Table 13

THE RESULTS FOUND IN THE FIFTH CASE BY ANSYS.

Parameter	The actual value of the machine	The improved values
rated current (In) (Calculated by Ansys)	2.91 A	2.61 A
starting current	12.78 A	11.60 A
rated torque	7.98 N.m	7.63 N.m
starting torque	36.01 N.m	35.61 N.m
starting torque/rated torque	4.51	4.41
rated rotating speed	96.18 rad/s	94.57 rad/s
Joule losses	256.76 W	226.74 W
iron losses	161.61 W	95.31 W
mechanical losses	6.91 W	6.71 W
total losses	425.28 W	328.76 W
efficiency	63.81%	69.52 %

In this case, the starting current of the DSIM decreases to 11.60 A. The nominal current takes a lower value than the previous one, with a decrease of 2.61A, which has a positive influence on reducing Joule losses. The iron losses decrease and reach a value of 95.31W, with a slight decrease in mechanical losses, resulting in an increase in motor efficiency, which reaches a value of 69.52%. In summary, in this case, the efficiency is the best compared to the other cases, with a lower starting current. However, this also leads to a decrease in starting torque and an increase in harmonics.

5.3 FINAL IMPROVED RESULS

A comparative analysis of the previously studied cases reveals that the observed improvements are mainly influenced by the following parameters:

- Outer diameter of the stator;
- Inner diameter of the stator;
- Slot geometry (slot height, b_{s1}, b_{s0});
- Air gap thickness;
- Conductor cross-sectional area used in the winding (copper wire).

The results of the design sensitivity analysis are presented as follows:

Table 14

Results of the Design Sensitivity Analysis.

The geometric parameters	The improved values	The electrical parameters	The improved values
outer diameter of the stator D_{ext}	143 mm	rated current	2.22 A
		starting current	10.09 A
inner diameter of the stator D_{int}	82 mm	rated torque	8.13 N.m
		starting torque	35.74 N.m
air gap		starting torque/ rated torque	4.39
maximum slot width b_{s2}	0.5 mm 5.49 mm	rated speed	92.37 rd/s
		Joule losses	218.23 W
minimum slot width b_{s1}	4.37 mm	iron losses	118.44 W
		mechanical losses	6.50 W
conductor cross-sectional area S_{co}	0.283 mm		
		total losses	343.07 W
stator slot opening b_{s0}	2.4 mm	efficiency	68.61 %
key height h_k	0.5 mm		
slot wedge height h_f	0.8 mm		
effective slot height	15 mm		
h_{ench}	12.5 mm		
height of rotor bars			

By adjusting the geometric characteristics of the machine while keeping the voltage and nominal power constant, significant performance improvements were observed during the analysis phase. The main findings are summarized as follows:

- Significant reduction in nominal current compared to the reference motor. This indicates better energy efficiency and a reduction in internal losses.

• Considerable decrease in starting current, which is an important parameter during machine startup. This can facilitate motor startup and reduce electrical stresses during this critical phase.

• Improvement in motor efficiency due to the reduction in total losses. Higher efficiency means better utilization of electrical energy and a decrease in thermal losses.

• Slight improvement in the machine's nominal torque.

This indicates an increased ability to provide constant torque at full load, which is essential for applications requiring high torque.

• However, there is a slight decrease in starting torque compared to the reference motor.

6. **CONCLUSION**

In this study, a detailed design sensitivity analysis of a 0.75 kW six-phase double-star induction machine was performed using ANSYS Maxwell. Each trial involved modifying a single geometric or electrical parameter to evaluate its influence on the machine's performance. The analysis identified configurations that enhance efficiency, reduce starting current, and lower manufacturing costs, demonstrating the effectiveness of systematic parameter variation in improving machine behavior.

This investigation provides valuable insight into the relationship between design parameters and performance, serving as a preliminary step toward more advanced mathematical optimization. Future work will focus on applying intelligent optimization algorithms and multiobjective techniques to further refine the machine design and validate the results experimentally.

ACKNOWLEDG(E)MENT(S)

The authors would like to acknowledge the support of the Direction Générale de la Recherche Scientifique et du Développement Technologique (DGRSDT).

CREDIT AUTHORSHIP CONTRIBUTION STATEMENT

Yacine Bendjeddou: conceptualization, methodology, machine construction, writing original draft.
Abdellatif Seghiour: investigation, writing, review & editing,
Mustapha Taib: supervision, resources, results curation.
Hemza Sellamna: visualization, writing, review & editing,
Abdelkader Tertag: simulation, formal analysis, writing original draft.
Noureddine Benouzza: supervision, resources, results curation, machine construction.

Received on 24 April 2025

REFERENCES

1. S. Guedida, B. Tabbache, K. Nounou, and M. Benbouzid, *Direct torque control scheme for less harmonic currents and torque ripples for dual star induction motor*, Rev. Roum. Sci. Techn. – Électrotechn. et Énerg., **68**, *4*, pp. 331–338 (2023).
2. M. Oussama, H. Lallouani, and B. Saad, *Direct torque control with space vector modulation using interval type 2 fuzzy logic regulators of dual star induction machine fed by two three-level neutral point clamped inverter*, Rev. Roum. Sci. Techn. – Électrotechn. et Énerg., **69**, *2*, pp. 159–164 (2024).
3. L. Wogi, A. Thelkar, T. Tahiro, T. Ayana, S. Urooj, and S. Larguech, *Particle swarm optimization-based optimal design of a six-phase induction motor for electric propulsion of submarines*, Energies, **15**, *9*, pp. 2994 (2022).
4. R. Chaudhary, A. Shahpatel, and S. Patel, *Optimal design of induction motor using genetic algorithm and comparison with conventionally designed induction motor*, IEEE International Conference on Power Electronics Intelligent Control and Energy Systems (ICPEICES), pp. 1–4 (2016).
5. B. Gecer, O. Tosun, H. Apaydin, and N.F.O. Serteller, *Comparative analysis of SRM, BLDC, and induction motor using ANSYS/Maxwell*, International Conference on Electrical, Computer, Communications and Mechatronics Engineering (ICECCME), pp. 1–6 (2021).
6. O. Tikhonova, I. Malygin, and A. Plastun, *Electromagnetic calculation for induction motors of various designs by "ANSYS Maxwell"*, International Conference on Industrial Engineering, Applications and Manufacturing (ICIEAM), pp. 1–5 (2017).
7. O.V. Tikhonova and A.T. Plastun, *Electromagnetic calculation of induction motor by "ANSYS Maxwell"*, IEEE Conference of Russian Young Researchers in Electrical and Electronic Engineering (EIConRus), pp. 822–826 (2018).
8. S. Bhattacharjee, *Analysis of a three-phase induction motor directly from Maxwell's equations*, American Journal of Physics, **80**, *1*, pp. 43–46 (2012).
9. E. Vassent, G. Meunier, A. Foggia, and G. Reyne, *Simulation of induction machine operation using a step-by-step finite element method coupled with circuits and mechanical equations*, IEEE Transactions on Magnetics, **27**, *6*, pp. 5232–5234 (1991).
10. R. Wang, H. Mohellebi, T.J. Flack, M.J. Kamper, J.D. Buys, and M. Feliachi, *Two-dimensional Cartesian air-gap element (CAGE) for dynamic finite-element modeling of electrical machines with a flat air gap*, IEEE Transactions on Magnetics, **38**, *2*, pp. 1357–1360 (2002).
11. Z. Maddi and D. Aouzellag, *Dynamic modelling of induction motor squirrel cage for different shapes of rotor deep bars with estimation of the skin effect*, Progress In Electromagnetics Research M, **59**, pp. 147–160 (2017).

.